Polymer 52 (2011) 866–873

Contents lists available at ScienceDirect

Polymer

journal homepage: www.elsevier.com/locate/polymer

Gel time prediction of multifunctional acrylates using a kinetics model

Aparna Boddapati, Santosh B. Rahane, Ryan P. Slopek, Victor Breedveld, Clifford L. Henderson, Martha A. Grover*

School of Chemical & Biomolecular Engineering, Georgia Institute of Technology, Atlanta, GA 30332-0100, United States

ARTICLE INFO

Article history:
Received 5 October 2010
Received in revised form
10 December 2010
Accepted 13 December 2010
Available online 21 December 2010

Keywords:
Photopolymerization
Gel time
Microrheology

ABSTRACT

A kinetics model for prediction of double-bond conversion and gel time in the photopolymerization of multifunctional acrylates is presented. The system consisting of a trifunctional acrylate, trimethylolpropane triacrylate (TMPTA), and a photoinitiator, 2,2-dimethoxy-1,2-diphenylethan-1-one (DMPA), was studied using Fourier-transform infrared spectroscopy (FTIR) measurements to monitor double-bond conversion and microrheology techniques to quantify the gel time for this system. Rate constants for the kinetics model were first estimated by fitting the model only to the FTIR double-bond conversion data, and later to both the FTIR and microrheology data. The measured gel time correlated with both the calculated initial rate of radical generation and a constant value of the predicted double-bond conversion, over a broad range of conditions. The model allows for materials formulation and exposure source intensity variables to be included in stereolithography inverse problem solutions, and could be applied to other cross-linking based photopolymerization systems.

1. Introduction

The photopolymerization kinetics of multifunctional acrylates has been studied extensively. These polymers are used in a wide array of applications ranging from lithography and coatings to biologically related uses such as dental composites and contact lenses [1]. The vinyl bonds on an acrylate react readily in the presence of radicals, and it is this fast rate of radical polymerization that makes acrylates attractive as compared to ionically polymerized monomers such as epoxides. In the case of multifunctional acrylates possessing multiple vinyl groups per monomer, reactions between distinct chains are prevalent. These types of reactions, known as cross-linking, bind different polymer chains in the reaction volume into a network. Cross-linking does not occur during photopolymerization of monofunctional monomers, thus resulting in a soluble collection of linear chains. In contrast, the cross-linked networks formed by multifunctional monomers are insoluble and this is known as the gel state. Polymers formed from the polymerization of pure monomers or mixtures including multifunctional acrylates are used in a wide range of applications. For example, several hydrogels that are used in tissue engineering are non-toxic derivatives of acrylates, and the cross-linking abilities of multifunctional acrylates are often exploited in these scenarios to achieve insolubility, high strength, and rigidity [2,3]. Moving beyond simple bulk multifunctional acrylate polymerization, the spatially controlled photopolymerization of multifunctional acrylates is the foundation on which stereolithography processes were developed. The significant durability of the gel networks formed by multifunctional acrylates is a desirable property in stereolithography applications, where polymer parts of various shapes and sizes are prepared using a computer generated exposure profile to selectively solidify a complex polymer shape in a vat of polymerizable monomer [4–7]. It is important to correctly understand and characterize the point at which gelation occurs (in space and time), because it will determine the geometry of the resulting polymer part.

Relating polymerization kinetics to solid part formation is challenging. To date, models to predict the height of cured parts take the form of analytical solutions to simplified kinetics—for example, deoxygenated systems with radical concentrations at constant steady-state levels [4]. In addition, measurements of the final part shape after removal from the resin vat may be influenced by part shrinkage during washing and drying steps, thus further confounding attempts to quantify the polymerization kinetics by solely measuring part height. This paper uses microrheology to obtain experimental data in support of our efforts to establish the relationship between polymerization kinetics and solid part height through more advanced kinetic models. Of particular importance here is the fact that microrheology can measure the location of the gel front throughout the polymerization process *in situ*, and is

* Corresponding author. Tel.: +1 404 894 2878; fax: +1 404 894 2866.
E-mail address: martha.grover@chbe.gatech.edu (M.A. Grover).

0032-3861/$ – see front matter © 2010 Elsevier Ltd. All rights reserved.
doi:10.1016/j.polymer.2010.12.024

therefore not impacted by shrinkage during washing or drying of the final part. The time point at which a resin transitions from a soluble liquid resin to an insoluble cross-linked network is called the gel time, and this parameter can readily be quantified experimentally through microrheology measurements [8–10].

In this paper, a model based on the kinetics of photopolymerization reactions of multifunctional acrylates is used to compute the gelation time for various cure conditions. First the experimental methods are presented, after which the kinetics model is documented in detail. This kinetics model is initially fit to the FTIR data only, after which the microrheology data are added to obtain a simultaneous fit of the rate constants and thus provide further model validation.

2. Experimental

2.1. Materials

Trimethylolpropane triacrylate (TMPTA, SR® 351) was obtained from Sartomer® and the photoinitiator 2,2-dimethoxy-1,2-diphenylethan-1-one (DMPA, IRGACURE® 651) was obtained from CIBA Specialty Chemicals®. The chemicals were used as received. In particular, the SR® 351 formulation of TMPTA contains 90–120 ppm of MEHQ, and this inhibitor was not removed. Experiments were performed on samples formulated with several different weight fractions of DMPA in TMPTA, and no additional solvent was added to these samples (Fig. 1).

2.2. FTIR procedure

Fourier-transform infrared spectroscopy was used to measure the double-bond conversion of the TMPTA over a range of times throughout the curing process. A sample holder was designed that enabled both UV curing and FTIR characterization on the same sample. This holder was made of two aluminum slabs, each with a 1 cm diameter aperture in the center. The slabs were used to align and contain two sheets of 65 μm thick polypropylene film, separated by a 100 μm thick Teflon® spacer to create a cavity. The cavity between the polypropylene films provides a thin and disposable sample chamber with rigid dimensions due to the Teflon® spacer and aluminum plates. The transmission characteristics of polypropylene enable sample illumination with UV light. Mixtures of initiator and uncured monomer were transferred into the sample chamber by pipetting the liquid samples along an open edge of the cell and allowing capillary action to fill the cavity. No attempts were made to remove oxygen from the TMPTA; rather, the TMPTA was assumed to be in equilibrium with the oxygen in the ambient environment. Three different initiator weight fractions were used for the FTIR measurements: 0.50%, 5.0%, and 10% DMPA. The entire sample holder was exposed to ultraviolet light from a Spectra-Physics

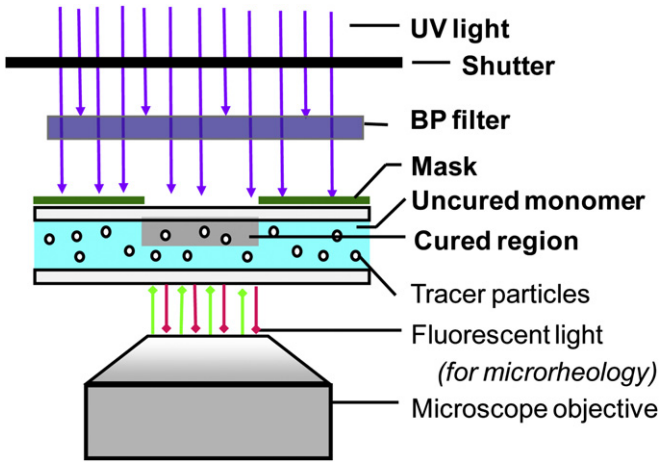

Fig. 2. Schematic of the cure setup used in the experiments and model.

1000 W Hg lamp through an IR water filter and bandpass filter (center wavelength 365 nm, full width at half-maximum 10 nm, peak transmission 55%), resulting in illumination at 365 nm and an intensity of 140 W/m^2. The exposure time of the samples was controlled via an electronic shutter (Uniblitz, Vincent Associates) that was operated through a customized LabView program for precise timing. A schematic of this setup is shown in Fig. 2.

Following UV irradiation for a controlled time period, FTIR measurements on the samples were performed *ex situ* using a Bruker FTIR (Bruker Vertex 80v) instrument operating in transmission mode. A total of 100 scans were collected for each sample at a resolution of 4 cm^{-1} to compile absorbance spectra. The double-bond conversion was calculated using the area under the C=C peak at 1625 cm^{-1}. Because the carbonyl content in the resin does not change during photopolymerization, the peak corresponding to asymmetric carbonyl stretching (C=O peak at 1720 cm^{-1}) was used as an internal standard in the FTIR analysis so that corrections could be made for slight variations in the cell path length. The peak area ratio (PAR) is defined as

$$\mathrm{PAR} = \frac{\mathrm{Area}_{1625\ \mathrm{cm}^{-1}}}{\mathrm{Area}_{1720\ \mathrm{cm}^{-1}}} \tag{1}$$

where $\mathrm{Area}_{1625\ \mathrm{cm}^{-1}}$ is the area under the C=C peak and $\mathrm{Area}_{1720\ \mathrm{cm}^{-1}}$ is the area under the C=O peak. Based on this peak area ratio, the double-bond fractional conversion α is calculated as

$$\alpha = 1 - \frac{\mathrm{PAR}}{\mathrm{PAR}_{t=0}} \tag{2}$$

where $\mathrm{PAR}_{t=0}$ is the initial value of the peak area ratio before any UV exposure.

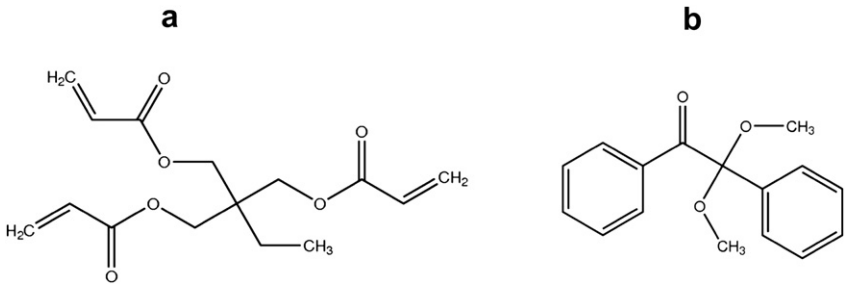

Fig. 1. (a) The trifunctional acrylate monomer SR®351, trimethylolpropane triacrylate (TMPTA); (b) the photoinitiator IrgaCure®651, 2,2-dimethoxy-1,2-diphenylethan-1-one (DMPA).

2.3. Microrheology

The gelation time of the TMPTA was measured via *in situ* particle tracking microrheology using the same optical setup that was used to illuminate samples for the FTIR experiments. Microrheology experiments were carried out under various exposure intensities, initiator concentrations, and with the focal plane of the microscope used to observe particle motion set at varying depths in the sample. The microrheology technique used in this work tracks the Brownian motion of individual 0.50 μm diameter fluorescent silica tracer particles using a high-resolution optical microscope (Leica DM-IRB), a CCD camera (Sentech STC-720) and frame grabber (Imagenation PCX-200AL), and image processing software (IDL, ITT VIS) to extract particle positions and reconstruct particle trajectories. In short, the "gel time" in microrheology experiments refers to the time at which a rapid change in the Brownian mobility of tracer particles is observed, indicating a sudden transition from a viscous liquid to an elastic network due to cross-linking of the trifunctional monomer [8].

Sample chambers of 120 μm thickness for the microrheology experiments were created by placing Parafilm spacers between two glass slides and slightly melting and cooling the Parafilm. A pipette was used to introduce the solution containing TMPTA, DMPA, and silica nanoparticles into the sample chamber. The concentration of tracer particles was extremely low (ca. 0.01 volume%) in order to facilitate tracking of individual tracers without affecting the optical properties of the sample. The sample was then exposed to UV, while simultaneously recording tracer particle motion at a well-defined focal plane in the sample. Further details on the experimental procedures for the microrheology measurements may be found in an earlier publication [8]. The specific experimental data points used in this paper for model comparison are given in Table 1, where I_0 is the incident intensity, [In] is the photoinitiator concentration, z is the depth into the sample from the top illuminated surface, and t_{gel} is the microrheology measured gel time.

3. Model

3.1. Rate equations

In this work, the reaction processes and time-dependent concentrations of various species typical in a radical photopolymerization process are modeled, including the concentrations of photoinitiator [In], radicals present [$R\cdot$], unreacted double bonds [DB], and oxygen [O_2]. The reactions considered in this work are:

$$\mathrm{In} \xrightarrow{k_d} 2R\cdot \tag{R1}$$

$$R\cdot + \mathrm{DB} \xrightarrow{k_p} R\cdot \tag{R2}$$

$$R\cdot + R\cdot \xrightarrow{k_t} R_{dead} \tag{R3}$$

$$R\cdot + \mathrm{O_2} \xrightarrow{k_{t,O_2}} R_{dead} \tag{R4}$$

where R_{dead} is any species produced that destroys one or more radicals.

The decomposition of the initiator is modeled as a first-order reaction with rate constant k_d. Two primary radicals are created per DMPA photoinitiator molecule [11,12], as shown in Reaction (R1). Once radicals have been formed in the system, the other three reactions (R2)–(R4) are assumed to be possible, which are modeled in this work with three additional rate constants: k_p for propagation of a radical through an acrylate double bond, k_t for termination between two radicals, and k_{t,O_2} for termination of a radical with an oxygen molecule. The termination reaction (R3) is a combination reaction, yielding a single species as the product. Vinyl monomers such as acrylates have been shown to terminate mostly via combination, rather than by disproportionation [13]. However, this assumption is not actually relevant for the modeling here, since this work does not involve modeling the molecular weight or concentration of polymer. Instead, the focus of this work is modeling the consumption of vinyl double bonds in the system, and it is this level of double-bond conversion that is used as a predictor of other polymer properties. It should also be noted that chain transfer reactions are not explicitly included here, but again such reactions would be of no consequence in terms of tracking the level of double-bond conversion in the system. In addition to the propagation and termination reactions, oxygen dissolved in the reaction volume can act as a radical scavenger, inhibiting both propagation and termination [14], and is thus explicitly included in the model.

Because we are using a multifunctional monomer, the double-bond conversion in the system is not proportional to the fraction of monomer consumed—the trifunctional monomer in polymer may still have one or two remaining unreacted double bonds. Thus, we model only the concentration of double bonds in the system, and not the concentration of free monomer, as is typical when modeling the reaction of linear polymers.

Given the four chemical reactions above, the following kinetics equations on the four species can be formulated:

$$\frac{d[\mathrm{In}]}{dt} = -k_d I(z)[\mathrm{In}] \tag{3}$$

$$\frac{d[R\cdot]}{dt} = 2k_d I(z)[\mathrm{In}] - 2k_t[R\cdot]^2 - k_{t,O_2}[R\cdot][O_2] \tag{4}$$

$$\frac{d[\mathrm{DB}]}{dt} = -k_p[R\cdot][\mathrm{DB}] \tag{5}$$

$$\frac{\partial[O_2]}{\partial t} = -k_{t,O_2}[R\cdot][O_2] + D_{O_2}\frac{\partial^2[O_2]}{\partial z^2} \tag{6}$$

Table 1
Microrheology data from Slopek [9].

Run	1	2	3	4	5	6	7	8	9	10	11	12
I_0 [W/m^2]	10	10	10	10	10	10	10	10	10	10	10	10
[In] [wt%]	5	5	5	5	5	5	8	6.5	5	4	3	2
z [μm]	112	106	68	44	20	8	60	60	60	60	60	60
t_{gel} [s]	9.0	8.8	7.3	6.0	4.3	3.8	5.3	5.8	6.7	7.5	8.8	11.5
Run	13	14	15	16	17	18	19	20	21	22	23	24
I_0 [W/m^2]	10	10	10	4	8	8	4	6	8	10	12	14
[In] [wt%]	1	0.5	0.25	2	2	1	2	2	2	2	2	2
z [μm]	60	60	60	60	60	60	60	60	60	60	60	60
t_{gel} [s]	17.3	26.7	41.2	22.5	11.7	20.2	22.5	14.0	11.7	9.8	8.1	7.3

Equation (6) is a partial differential equation, in which we explicitly model the diffusion of oxygen within the resin sample in the vertical direction, the only direction in which concentration gradients can develop. Due to its high diffusivity in TMPTA, the oxygen may diffuse from uncured top layers of the sample chamber down to the curing front, competing with double bonds for radicals and significantly slowing down the conversion rate and gel time. The chamber is sealed by the two glass slides, and thus insulating boundary conditions are applied at both the upper and lower ends of the simulation domain. The local illumination intensity is $I(z)$, which deviates from the incident intensity I_0 due to the absorption by the resin.

3.2. Parameterization of the model

There are four unique rate constants in the kinetics model, plus the diffusivity of oxygen in TMPTA. The values of the physical parameters used in the model presented in this work are shown in Table 2.

The decomposition kinetics of a photoinitiator into initiator radicals are typically modeled using the first-order rate constant [19]

$$k_d = \frac{2.3\phi\varepsilon\lambda}{N_A hc} \tag{7}$$

where $0 < \phi < 1$ is the quantum efficiency of the photoinitiator, N_A is Avagadro's number, h is Planck's constant, and c is the speed of light. The molar absorptivity of the resin, ε, depends upon the source wavelength λ. If $\phi = 1$, each photon absorbed triggers a single decomposition reaction to generate the desired initiator radical(s) product. The overall rate of initiator decomposition R_i is modeled by multiplying the rate constant k_d by the initiator concentration [In] and the local intensity (I):

$$R_i = k_d I(z)[\mathrm{In}] \tag{8}$$

$$I(z) = I_0 \exp\{-2.3\varepsilon z[\mathrm{In}]\}$$

The incident intensity at $z = 0$ is I_0, but within the sample at $z > 0$, the intensity will be attenuated, due to absorption of the light in the resin. Beer's law was used along with the molar absorptivity ε to yield the rate of initiator decomposition at depth z.

The TMPTA rate constants for propagation and termination have been estimated at elevated temperatures and lower values of R_i than those considered here [20,21]. The rate constant for oxygen termination k_{t,O_2} is often expected to be faster than k_t, due to some combination of a higher intrinsic reactivity of oxygen with a radical as compared to the vinyl double bond or to a higher diffusivity for oxygen in the resin than the monomer itself [22,23]. In the study here we do not assume specific values of k_p, k_t, and k_{t,O_2} *a priori*, but instead fit them to the experimental data and discuss the values in the context of available estimates in the literature.

The diffusivity of oxygen in TMPTA has been estimated [17], as noted in Table 2. The diffusion length $L = \sqrt{D_{O_2}\tau}$ can be computed as $L = 50$ μm for a time scale $\tau = 30$ s, which is one of the longer gel times recorded in our study. Compared to a cell depth of 100 μm, diffusion of oxygen could therefore be significant over the experimental timescales, although it is not so fast as to create a uniformly well-mixed environment either. Therefore, oxygen diffusion has been explicitly modeled and included in this work. The diffusion of DMPA in TMPTA is expected to be significantly slower due to its higher molecular weight, and thus its diffusion is not included in Equation (4) of the kinetics model.

All calculations were performed using MATLAB®. The resin sample was discretized vertically into slices of thickness $\Delta z = 5$ μm. The spatial second derivative for the oxygen diffusion was approximated using a centered finite difference method, with insulated top and bottom surfaces representing the glass slides sealing the top and bottom surfaces. Integration of the resulting ordinary differential equations was performed using the built-in function `ode23s`. The function minimization to fit the rate constants was implemented using the `patternsearch` function in MATLAB®.

Table 2
Physical parameters used in the kinetics model. Values given are for the initiator DMPA and the monomer TMPTA.

Variable	Description	Value	Units	Reference
ρ_{mon}	Density of monomer	1.1×10^6	g/m^3	
MW_{mon}	Molecular weight of monomer	296	g/mol	
MW_{init}	Molecular weight of initiator	256	g/mol	
λ	Wavelength of light source	365	nm	
ε	Molar absorptivity of initiator at wavelength λ	15	m^2/mol	[15]
ϕ	Quantum efficiency of initiator	0.6	–	[16]
D_{mon,O_2}	Diffusivity of oxygen in monomer	1.0×10^{-10}	m^2/s	[17]
$[O_2]_0$	Initial concentration of oxygen in TMPTA, at equilibrium with ambient air	1.05	mol/m^3	[18]

4. Results

Of the four rate constants used in the model, the initiator dissociation rate constant has been the most thoroughly documented in the literature. Here we use the nominal value for k_d calculated from Eq. (7) using the physical constants reported in Table 2 and fit the remaining three rate constants using several different assumptions.

4.1. Fit to FTIR conversion measurements

A simultaneous fit was made to TMPTA double-bond conversion data from two sources: the measurements of Lee et al. [24] which used *in situ* FTIR under deoxygenated conditions, and the *ex situ* FTIR measurements made in this work in the presence of ambient oxygen levels, as described in Section 2. A subsequent dark reaction following UV irradiation is modeled for the oxygenated data sets collected in this work since it is an *ex situ* measurement that occurs on the time scale of minutes after the initial exposure is completed. In this case, the dark reaction was simulated for 60 s, after which it was found that all radicals in the model have terminated. The diffusion of oxygen within the resin is also included in the model predictions. The conditions used for the deoxygenated data set are similar to the oxygenated experiments, with incident intensity $I_0 = 140$ W/m^2 at the wavelength $\lambda = 365$ nm, and a DMPA concentration of 1.0 wt%. Lee et al. used a sample thickness of 15 μm, much thinner than the 120 μm sample described in Section 2.

The best-fit values for the three rate constants $\{k_p, k_t, k_{t,O_2}\}$ are found by minimizing the sum squared error (SSE) between the FTIR experimental measurements and model-predicted double-bond conversion:

$$\mathrm{SSE}_{\mathrm{FTIR}} = \sum_{i=1}^{2}\left(\frac{1}{n_{t,i}}\sum_{j=1}^{n_{t,i}}\left(\alpha_{j,i}^{\mathrm{meas}} - \alpha_{j,i}^{\mathrm{pred}}(k_p, k_t, k_{t,O_2})\right)^2\right) \tag{9}$$

Here the index j denotes the double-bond conversion α at the jth time point (in experiment i). Since there are two experimental studies used in this fit, the quantity SSE_{FTIR} is thus the sum of the two average sum squared errors. The number of data points in experiment i is $n_{t,i}$.

The motivation for building the kinetics model presented in Equations (3)–(6) is to incorporate more chemical detail relevant for radical polymerization at early conversion, such that the gel time or exposure dose required to form a gel can be predicted as a function of the sample composition and processing conditions. Thus, only the data points at early conversion were used in fitting the rate constants, and consequently the model predictions will only be accurate for early conversion prior to gelation.

The best-fit values for the rate constants are $\{k_p, k_t, k_{t,O_2}\} = \{0.498, 1.30, 2.11\}$ m^3/mol s, and the corresponding predictions are shown in Fig. 3. Only the points marked with 'x's were used in the fit. In the Lee data shown in Fig. 3(a), only points up to 15% conversion were used in the fit, which establishes a clear slope consistent with a constant value of $k_p/\sqrt{k_t}$, as expected for deoxygenated systems with constant values of the rate constants [4]. Beyond this point, the slope of the conversion curve begins to decrease, consistent with increasing viscosity as the polymerization continues to proceed toward imminent gelation. In the oxygenated data set of Fig. 3(b), the data points up to 5 s were included for the lowest weight fraction of initiator (0.5 wt% DMPA). An initial transient is apparent up to 2 s, which is expected due to the presence of oxygen that quenches radicals and prevents significant polymerization until it is consumed. Thus the additional 3 s of data was included in the fit to capture the upturn in the conversion beyond this initial slower startup period. At the higher initiator weight fractions, the *ex situ* measurements did not have the time resolution to capture lower conversions, so the first point was included from the 10% DMPA experiment, and the first two points for 5% DMPA, in order to represent the fast kinetics observed for these high initiator loadings. When the data for 5% or 10% DMPA were not included in the fit, a lower value of $k_p/\sqrt{k_t}$ was computed, and the predictions for 5% and 10% DMPA were significantly slower, inconsistent with the data in Fig. 3(b).

Overall, the model predictions shown in Fig. 3 compare well to the experimental measurements at early conversion, using a single set of rate constants for both data sets. At longer times, the system gels, preventing full conversion to be achieved, while the constant values of the rate constants in the model will allow for predictions of 100% conversion as possible. The constant slope in the deoxygenated data is well predicted by the model ($k_p/\sqrt{k_t} \approx 0.44$). In the oxygenated data set of Fig. 3(b), the conversion rate is slightly overestimated at the low DMPA loading level, while slightly underestimating the high loadings.

We do not argue here that this set of rates is unique. For example, as long as the quantity of $k_p/\sqrt{k_t}$ is maintained constant, k_p and k_t can be varied over a significant range, with little impact on the conversion predictions. However, for values of k_p much less than 0.1, there would not be significant polymerization on the timescales of the experiments, which is inconsistent with the data.

4.2. Joint fit to conversion from FTIR and gel time from microrheology

The objective in this study is not simply to predict conversion, but rather to use a physically realistic model to predict the gelation time at which the liquid monomer is converted into a solid gel. In previous polymerization studies, monomer conversion has frequently been used as a predictor of gelation. For example, Flory provides a criterion for gelation in step condensation polymerization based on the conversion α and monomer functionality f—only beyond a critical conversion α_c can a percolating gel network be formed [25].

$$\alpha_c = \frac{1}{f-1}$$

For our trifunctional monomer, a maximum of $f = 6$ branches can be formed in a radical polymerization, so $\alpha_c = 20\%$. This expression assumes no cycle formation, while a modified version assumes equal probability of cycle formation

$$\tilde{\alpha}_c = \frac{1}{\sqrt{f-1}}$$

and for $f = 6$ yields $\tilde{\alpha}_c = 44\%$. Here we are dealing with a concentrated monomer, so cyclization may be less important than a dilute monomer in solvent. However, the chains are initially growing in isolation, and cycle formation cannot be ruled out either. More significantly, these expressions are derived for step condensation, but the kinetics of radical polymerization incorporates multiple reaction species and events. Critical conversion arguments have also been used for multifunctional acrylate radical polymerization, and the final expressions depend upon the individual rate constants for termination, initiation, and propagation [4]. Similar approaches have recently been developed for living radical polymerization [26]. However, in both cases a steady-state radical concentration is assumed, and neither the oxygen termination nor oxygen diffusion is included. Despite the complexities of

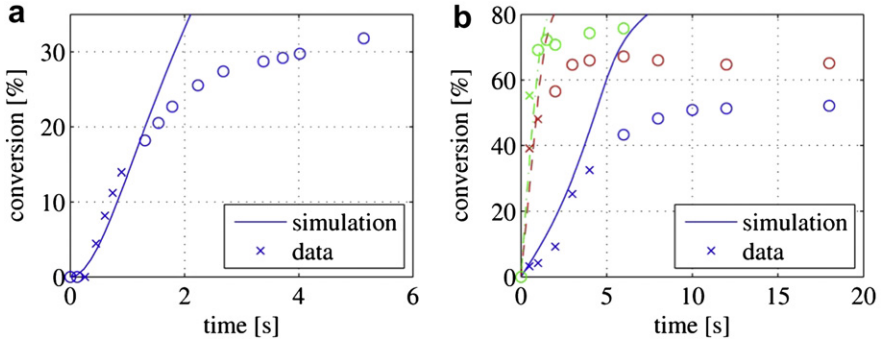

Fig. 3. Conversion data by FTIR, along with the model-predicted conversions α. The three rate constants used here were fit to the FTIR data only: (a) deoxygenated conditions and (b) oxygenated conditions. The 'x's represent data points used in the fit, and the 'o's are data points not used to fit the rate constants. In (b), the blue solid curve and symbols are for 0.5 wt% DMPA, the red dashed curve denotes 5 wt% DMPA, and the green dashed-dot curve is 10 wt% DMPA. (For interpretation of the references to colour in this figure legend, the reader is referred to the web version of this article).

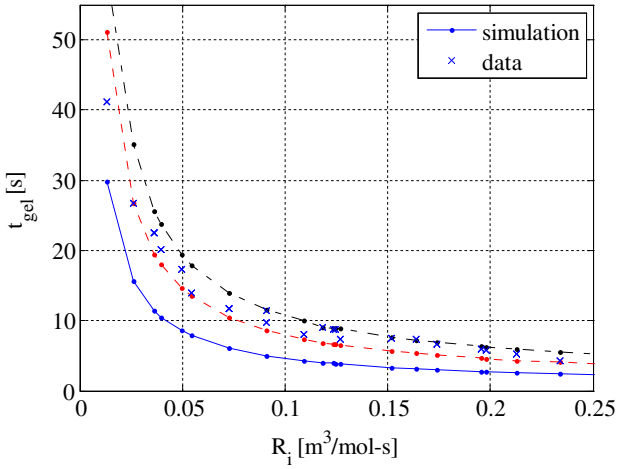

Fig. 4. Plot of microrheology data, and simulated curves with different conversion cutoffs: 10% (blue solid), 20% (red dashed), 30% (black dashed-dot). The rate constants used in the simulation were fit to the FTIR data: $\{k_p, k_t, k_{t,O_2}\} = \{0.498, 1.30, 2.11\}$ m^3/mol s. (For interpretation of the references to colour in this figure legend, the reader is referred to the web version of this article.)

the kinetics, the concept of using a critical conversion for predicting gelation might still be appropriate. Therefore, it was decided to experimentally determine if a single critical conversion criterion could be established for this system.

Here gelation is defined as the time at which the liquid monomer is converted into a solid gel. This transition was measured via microrheology as a sudden drop in the local particle mobility. It was hypothesized in this work that the gel time t_{gel} at a particular position in the vat should depend strongly upon the local initial rate of radical generation R_i. Therefore the rate constants estimated from the FTIR data were used to compute R_i for each of the 24 experimental data points in Table 1. In Fig. 4, the measured gel time t_{gel} is plotted versus R_i, and in fact does fall along a single curve, within an experimental variation of 1 s. Apparently the quantity R_i alone is sufficient to predict the gel time in this system. Of course, R_i depends on many quantities, including the depth in the sample, the initiator weight percent, and the intensity and wavelength of the UV source. This data suggests a simpler design principle, in which any single process setting can be used to vary R_i, and thus the value of t_{gel} at each point in the resin sample. Conversely, to obtain a particular t_{gel} at a desired depth z in the vat, either the intensity I_0 or the initiator concentration [In] may be adjusted to achieve the corresponding value of R_i.

Slopek [9] also reported microrheology measurements for deoxygenated samples, which form gels much more rapidly—at times less than 5 s for all $R_i > 0.05$ mol/m^3 s. It is difficult to draw a definitive conclusion about this deoxygenated data set, due to the limited experimental resolution, but the data did not appear to fall along a single curve on the t_{gel}–R_i plot. Additional unmodeled effects, such as heat release, molecular weight-dependent rate "constants" or residual oxygen levels, might need to be included in the model to accurately predict t_{gel} in such cases. Instead, here we focus on predicting the gel time in the presence of ambient oxygen, which is of more practical relevance for stereolithography.

The goal of this work is to use the kinetics model to predict gel time or gelation dose of illumination so that inverse process design problems like stereolithography might be more accurately solved, even though the kinetics model defined and discussed earlier in this paper only predicts double-bond conversion, as shown in Fig. 3, along with the concentrations of initiator, radical, and oxygen. Viscosity is often modeled as a function of molecular weight, but this dependence was not incorporated into the kinetics model used here for simplicity and to avoid overfitting. Flory predicted a critical value of the double-bond conversion, after which gelation is possible [25], so it was hypothesized in this work that TMPTA double-bond conversion might be correlated with gel time. If such a relationship is valid, then it would provide the connection needed to utilize the kinetic model for predicting the required gelation dose in applications such as stereolithography.

The results of investigating constant double-bond conversion criteria for fitting the microrheology gel time data are shown by the curves in Fig. 4, denoting the times at which 10%, 20%, and 30% conversion was reached, at each of the 24 settings used in the microrheology experiments. Because microrheology is an *in situ* measurement, no dark reaction is included in the simulations, but the effect of oxygen diffusion is included. The lines connecting the 24 modeled points are used only to guide the eye. A strong correlation between the data and the model predictions is evident, and the conversion cutoff of 20% appears to provide the best agreement. The point with the largest disagreement is at the smallest value of R_i, as the curves asymptotically approach infinity.

The rate constants used in the simulations in Fig. 4 were computed using only the FTIR data, and they are not necessarily unique. It might be possible to improve their estimates by performing a simultaneous fit to both the FTIR and microrheology data. This simultaneous fit could add insight into the fundamental rate constants and underlying phenomena; it could also allow for better fitting of the microrheology data for t_{gel} using a conversion cutoff α_{cut}. To perform this simultaneous fit, we defined the average squared error over the set of 24 microrheology measurements as

$$\mathrm{SSE}_{\mu rh} = \frac{1}{24}\sum_{i=1}^{24}\left(t_{gel,i}^{meas} - t_{gel,i}^{pred}\right)^2 \tag{10}$$

and then computed the three rate constants to minimize $\mathrm{SSE}_{FTIR} + \mathrm{SSE}_{\mu rh}$.

The best-fit rate constants are shown in Table 3, for the three different conversion cutoffs shown in Fig. 5 along with two additional intermediate values. The values obtained by fitting only to the FTIR data are shown in the first row for comparison. The numerical values of the sum squared fitting errors are also given in the table. Several observations can be made from Table 3. Including the microrheology data in the fit does not dramatically change k_p or k_t, and thus $k_p/\sqrt{k_t} \sim 0.44$ for all cases in the table. The sum

Table 3
Rate constants and average sum squared error for various fits to the experimental data.

α_{cut} [%]	k_p [m^3/mol s]	k_t [m^3/mol s]	k_{t,O_2} [m^3/mol s]	$k_p/\sqrt{k_t}$	SSE_{FTIR}	$\mathrm{SSE}_{\mu rh}$	$\mathrm{SSE}_{FTIR} + \mathrm{SSE}_{\mu rh}$
–	0.498	1.30	2.11	0.438	106.5	–	–
10	0.535	1.60	3.11	0.423	117.4	22.6	139.9
15	0.533	1.49	2.56	0.437	109.0	10.1	119.1
20	0.504	1.31	2.06	0.440	106.6	6.8	113.4
25	0.493	1.26	1.74	0.439	108.8	7.9	116.7
30	0.502	1.30	1.56	0.441	113.4	12.3	125.7

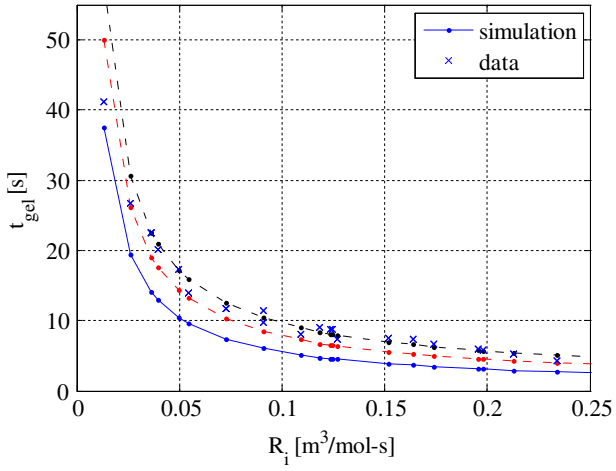

Fig. 5. Plot of fits for three conversion cutoffs: 10% (blue solid), 20% (red dashed), 30% (black dashed-dot). The rate constants used in each fit were optimized for that particular value of the conversion cutoff. (For interpretation of the references to colour in this figure legend, the reader is referred to the web version of this article.)

squared error for the FTIR term is expected to increase when the microrheology data is included in the fit, due to the tradeoff in fitting to more data points. However, this increase is slight, and for the 20% conversion cutoff value there is virtually no loss of accuracy in the FTIR prediction. The conversion cutoff of 20% provides the best overall accuracy among the five cutoff values, having the smallest microrheology fitting error, as can be seen in Fig. 5. The cutoffs of 15% and 25% are nearly as good.

The simulation results shown in Fig. 5 are similar to those in Fig. 4, because the rate constants did not change substantially among the various fits. The three curves in Fig. 5 are somewhat closer together, compared to Fig. 4, since their rate constants are now optimized to fit the gel time data. Note that the value of $k_p/\sqrt{k_t} \sim 0.44$ changed very slightly as the conversion cutoff was changed. The slope on the deoxygenated FTIR data is strongly sensitive only to this quantity, so that it would be difficult to achieve a good overall fit to the FTIR and microrheology data without having $k_p/\sqrt{k_t} \sim 0.44$.

The change in conversion cutoff was compensated in the optimization by a slight change in the value of the oxygen termination rate constant: as the conversion cutoff was raised, the value of k_{t,O_2} decreased by 50%. The effect of this decrease on the kinetics is that fewer radicals are terminated by oxygen early in the cure process, thus prolonging the time during which oxygen is present and ultimately speeding the polymerization. This effect was particularly important for the smallest value of R_i, as can be seen by comparing Figs. 4 and 5.

5. Discussion

As mentioned previously, the rate constants obtained from this fit are not necessary unique. The value of the oxygen termination rate and value of $k_p/\sqrt{k_t}$ are both local minima in the sum square errors indicating a unique fit, while the exact values of k_p and k_t could not be uniquely estimated. Adding the microrheology data to the FTIR data does not provide the additional information needed to better estimate the "true" values of the rate constants, nor does it contradict the values of the rate constants obtained solely from the FTIR data. However, adding the microrheology data to FTIR data does suggest that our FTIR-estimated rate constants are predictive for computing both conversion and gel time.

Constant values were estimated for the three rate constants, even though they are expected to depend on the viscosity. More specifically, the viscosity approaches infinity as the system approaches the gel point. However, Anseth et al. found that $k_p/\sqrt{k_t}$ for TMPTA is approximately constant up to the highest measured value at 14% conversion [21]. This is also consistent with observations in the microrheology experiments. The viscosity is approximately constant, and then increases rapidly when the system approaches gelation. The time of this transition is the gel time as measured by microrheology.

The values of the rate constants for TMPTA can be compared to kinetic parameterizations in previous studies. Anseth et al. determined rate constants for TMPTA using experimental results from a photo differential scanning calorimeter (DSC), including a dependence on free volume [21]. They applied the steady-state analysis for radical concentration during continuous irradiation of the resin to obtain the ratio $k_p/\sqrt{k_t}$ as a function of the propagation rate (measured through the DSC). By turning the UV source on and off, non-steady-state analysis was applied to separately estimate the ratio k_p/k_t, thus enabling independent estimates of k_p and k_t. They estimated $k_p = 0.4\ \mathrm{m^3/mol\ s}$ and $k_t = 100\ \mathrm{m^3/mol\ s}$ at the low conversion limit, yielding a value of $k_p/\sqrt{k_t} = 0.04\ (\mathrm{m^3/mol\ s})^{0.5}$. This value of k_p is consistent with ours in Table 3 ($k_p = 0.5\ \mathrm{m^3/mol\ s}$), while our value of $k_t = 1.3\ \mathrm{m^3/mol\ s}$ is significantly lower. There are two notable differences between our experimental conditions. First, the experiments in Anseth et al. [21] were conducted at 30 °C, while ours were at ambient temperature. Moreover, their value of radical generation rate is $R_i < 0.002\ \mathrm{m^3/mol\ s}$, which is an order of magnitude below our range of $0.02 < R_i < 0.23\ \mathrm{m^3/mol\ s}$ as seen in Figs. 4 and 5. Termination, and even the overall mode of polymerization and cross-linking, may be very different in different R_i regimes. Our model presented here represents a range of R_i that is of practical interest for stereolithography, but it is not necessarily valid outside that range.

Given our estimate of the conversion cutoff of 20%, we can re-evaluate the FTIR conversion data in Fig. 3(a) and (b). At a conversion of 20%, the conversion is still increasing rapidly in both sets of experiments. While this might at first appear inconsistent with gelation, that is not necessarily the case. Conversion will not immediately halt at gelation, but rather the mobility of polymers will cease, hindering both propagation and termination. In fact, termination will slow down first, since two radicals must find each other to terminate, and many radicals will be attached to polymer. Propagation can continue more readily, since the primary radicals and monomer can diffuse through the gel. Thus, Fig. 3 does not contradict our conclusion, since the turn-over in the conversion curves is expected during *or after* gelation. For consistency and completeness we also used Equation (8) to compute the initial rate of radical generation R_i in the FTIR data, which is slightly higher than for the microrheology data. For example, with the Lee conditions [24] at 1 wt% DMPA, we obtain $R_i = 0.38\ \mathrm{mol/m^3\ s}$ at the incident surface, and $R_i = 0.33\ \mathrm{mol/m^3\ s}$ at $z = 100\ \mu\mathrm{m}$, compared to a maximum value of $R_i = 0.23\ \mathrm{mol/m^3\ s}$ in the microrheology data set.

The gel time predictions of the kinetics model presented here are not necessarily more accurate than other alternative modeling approaches. For example, a simpler model can be fit as $R_i\, t_{gel} = 0.95$. Assuming that R_i is approximately constant over the irradiation time, this model implies that the system gels once a fixed number of radicals have been generated. While this is interesting to note, and simple to compute, it is not as accurate as the kinetics model. An alternative approach is to build an E_c–D_p model [27]. While this model is also very simple to evaluate, its two model parameters are

fit to experimental data for a fixed initiator concentration, irradiation intensity, and wavelength, so it is not useful for gaining insight into the underlying chemistry, or for designing a new process and recipe. The kinetics model presented here can be used to design the resin formulation and intensity profile for stereolithography of TMPTA with DMPA, over a wide range of conditions and gel times. It could also be applied to other initiators and multifunctional monomers. Moreover, it could be used to determine the desired properties of a monomer and an initiator, which would then enable the rational selection of the chemical or even enable molecular design of a new monomer with novel chemical reactivity.

6. Conclusions

A kinetics model was presented to predict conversion and gel time as a function of the process conditions and the chemical composition of the resin. The model was validated using the trifunctional monomer TMPTA and the photoinitiator DMPA. Conversion data was obtained from FTIR measurements, and gel time data from microrheology. The gel time could be uniquely predicted using only the initial value of radical generation, as predicted by the kinetics model. The data spanned over gel times from 5 s to 50 s, corresponding to an order of magnitude in both irradiation intensity and initiator concentration. This simple design rule relating R_i to gel time can now be used to select process conditions and sample recipe for applications of TMPTA and DMPA in stereolithography. In addition, the relationship between the radical generation rate and the gel time was correlated with a constant value of the double-bond conversion. It also suggests that these results may have further applicability to other monomer and initiator systems.

Acknowledgments

The authors gratefully acknowledge financial support from CIBA VISION®, and greatly appreciate helpful discussions in their collaboration with David Rosen, Amit Jariwala, and Fei Ding.

References

[1] Bowman CN, Peppas NA. Chemical Engineering Science 1992;47(6):1411–9.
[2] Goodner MD, Bowman CN. Chemical Engineering Science 2002;57(5):887–900.
[3] Nguyen KT, West JL. Biomaterials 2002;23(22):4307–14.
[4] Lee JH, Prud'homme RK, Aksay IA. Journal of Materials Research 2001;16(12):3536–44.
[5] Tang YY, Henderson C, Muzzy J, Rosen DW. International Journal of Materials & Product Technology 2004;21(4):255–72.
[6] Zhang X, Jiang XN, Sun C. Sensors and Actuators A – Physical 1999;77(2):149–56.
[7] Flach L, Chartoff RP. Polymer Engineering and Science 1995;35(6):483–92.
[8] Slopek RP, McKinley HK, Henderson CL, Breedveld V. Polymer 2006;47:2263–8.
[9] Slopek R. In-situ monitoring of the mechanical properties during the photopolymerization of acrylate resins using particle tracking microrheology. Ph.D. thesis. Atlanta, GA: Georgia Institute of Technology; 2008.
[10] Winter HH, Chambon F. Journal of Rheology 1986;30(2):367–82.
[11] Pappas SP, Asmus RA. Journal of Polymer Science. Polymer Chemistry Edition 1982;20(9):2643–53.
[12] Szablan Z, Lovestead TM, Davis TP, Stenzel MH, Barner-Kowollik C. Macromolecules 2007;40:26–39.
[13] Moad G, Solomon DH. Termination. The chemistry of radical polymerization. Oxford: Elsevier; 2006. p. 233–78.
[14] Decker C, Jenkins AD. Macromolecules 1985;18(6):1241–4.
[15] Berchtold KA, Lovestead TM, Bowman CN. Macromolecules 2002;35(21):7968–75.
[16] Goodner MD, Bowman CN. Modeling and experimental investigation of light intensity and initiator effects on solvent-free photopolymerization. In: Long TE, Hunt MO, editors. National meeting of the American chemical society, vol. 713. Las Vegas, Nevada: American Chemical Society; 1998. p. 220–31.
[17] O'Brien AK, Bowman CN. Macromolecules 2006;39(7):2501–6.
[18] Gou LJ, Coretsopoulos CN, Scranton AB. Journal of Polymer Science Part A – Polymer Chemistry 2004;42(5):1285–92.
[19] Odian G. Radical chain polymerization. Principles of polymerization. New York: John Wiley & Sons; 2004. p. 198–349.
[20] Anseth KS, Wang CM, Bowman CN. Macromolecules 1994;27:650–5.
[21] Anseth KS, Wang CM, Bowman CN. Polymer 1994;35(15):3243–50.
[22] Fouassier JP, Merlin A. Journal of Photochemistry 1980;12(1):17–23.
[23] Neta P, Huie RE, Ross AB. Journal of Physical and Chemical Reference Data 1990;19(2):413–513.
[24] Lee TY, Kaung W, Jonsson ES, Lowery K, Guymon CA, Hoyle CE. Journal of Polymer Science Part A – Polymer Chemistry 2004;42(17):4424–36.
[25] Flory PJ. Journal of the American Chemical Society 1941;63:3083–90.
[26] Irzhak TF, Irzhak VI. e-Polymers 2010;118:1–21.
[27] Zissi S, Bertsch A, Jezequel J-Y, Corbel S, Lougnot DJ, Andre JC. Microsystem Technologies 1995;2(1):97–102.